# Controlling the Energy Transfer in Lanthanide-Organic Frameworks for White-Light Emitting Materials Production

**Leonis L. da Luz [a], Bárbara F. Lucena Viana [b], Gabriel C. Oliveira da Silva [b], Claudia C. Gatto [b], Adriana M. Fontes[c], Marcos Malta[c], Ingrid T. Weber [b], Marcelo O. Rodrigues [b]* and Severino Alves Júnior [a]**

[a] *Departamento de Química Fundamental, UFPE, 50670-901, Recife, PE, Brazil. Tel. +55 81 2126-7475; Fax: +55 81 2126-8442; E-mail: salvesjt@ufpe.br*
[b] *Instituto de Química, Universidade de Brasília, 70910-900, Brasília – DF, Brazil. Tel. +55 61 3107-3876; Fax: +55 61 3273-4149; E-mail: marcelozohio@unb.br*
[c] *Instituto de Química, Universidade Federal da Bahia, Campus Ondina, Salvador (BA), Brazil. Fax: 55 71 3237 4117; Tel: 55 71 3283 6850;*

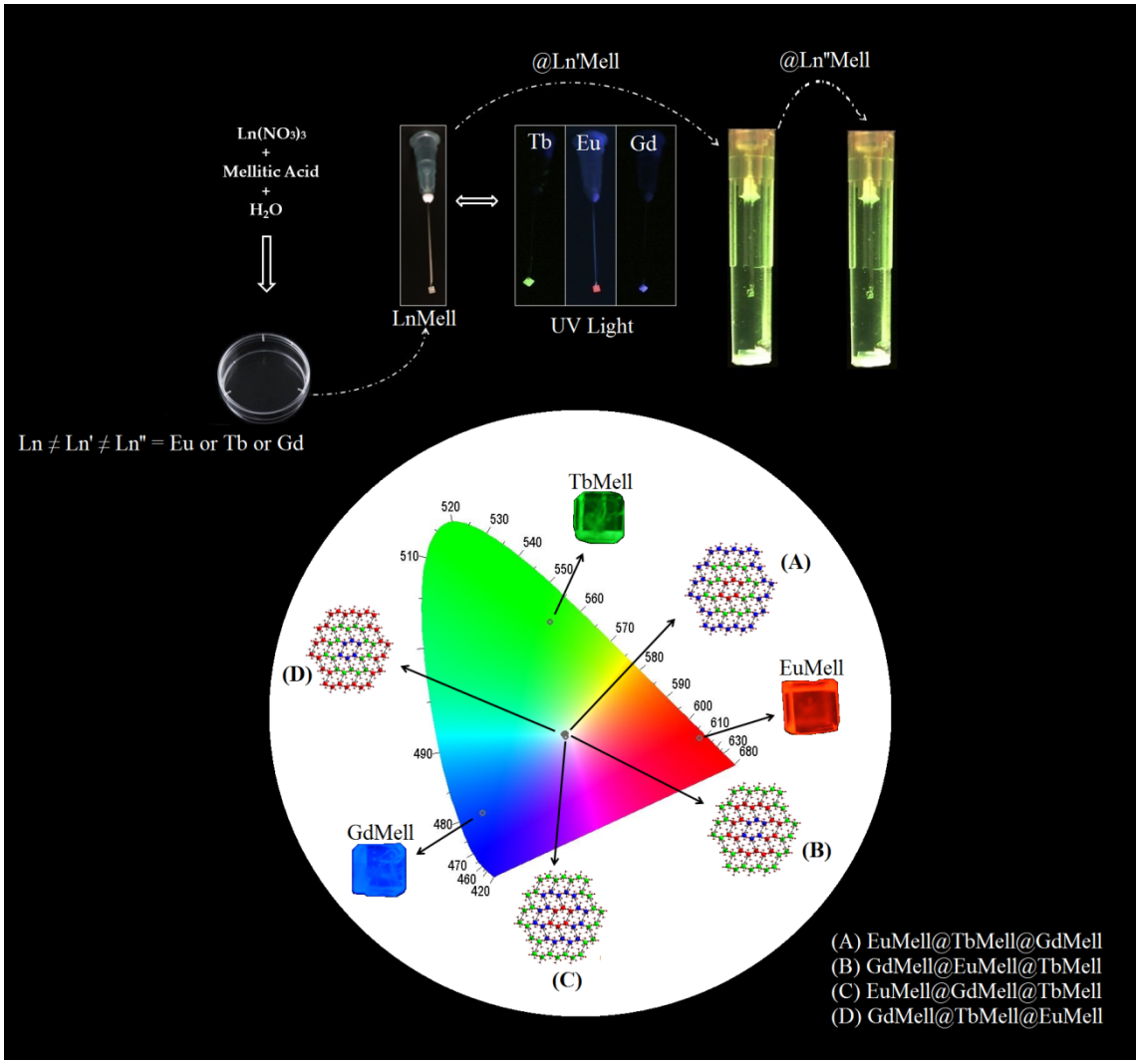

**SUMMARY:**

**Experimental Detail**

**Chemicals**

Mellitic acid and lanthanide oxides (99.99%) were purchased from Aldrich and used without further purification. $[Ln(NO_3)_3 \cdot 6H_2O]$ (where $Ln^{3+} = Eu^{3+}$, $Tb^{3+}$ and $Gd^{3+}$) were obtained by reaction of nitric acid with the corresponding lanthanide oxide.

**Experimental Procedure**

Synthesis of $[Ln_2(Mell)(H_2O)_8]$ seed crystals, 0.85 mmol of $[Ln(NO)_3 .6H_2O]$ (99,99%, Sigma-Aldrich) and 0.85 mmol of Mellitic Acid ―Mell (98%, Sigmal-Alfrich) were dissolved in $H_2O$ ultrapure to 8,5 mL of soluction and stirred for 2 minutes. The reaction mixture was placed in a Petri dish (60 mm of diam. × 15 mm of H) and kept at room temperature. Colorless crystals suitable to X-ray diffraction were obtained after 15 days. Selected single-crystals, *R-MOF, G-MOF* or *B-MOF* (cores), were supported on the hypodermic needles and immersed in the protective needle caps containing 200 µL unreacted solution of different lanthanide ion and ligand precursor. The subsequent layers were growth during 3 days (Figure S1).

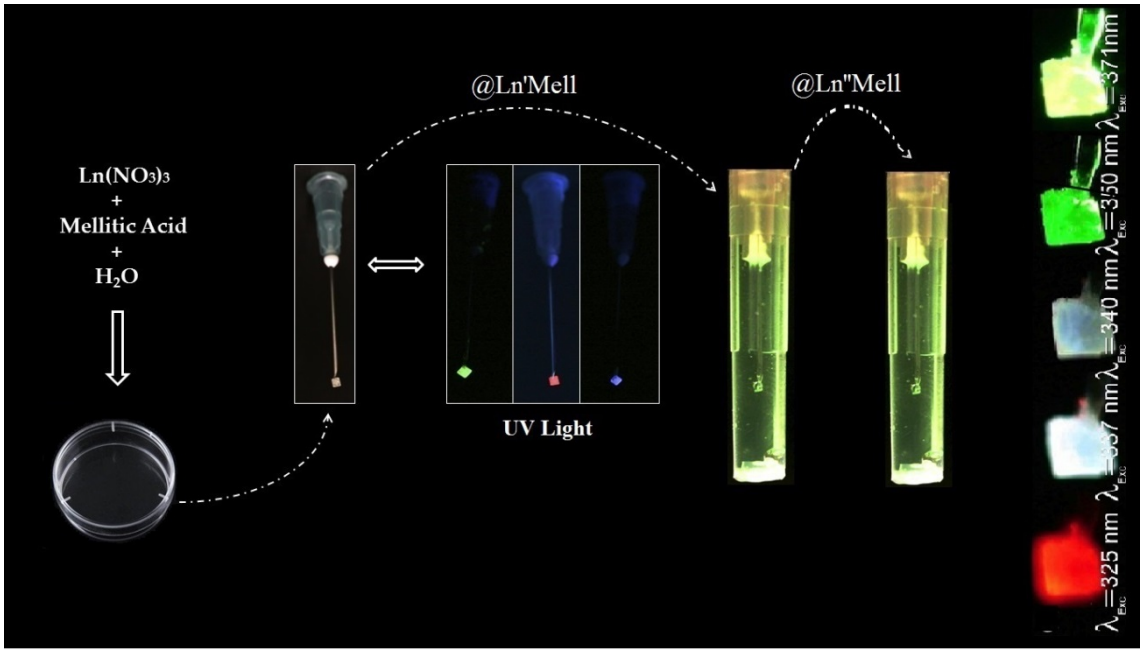


**Figure S1:** Schematic representation of the epitaxial growth.

**General Instrumentation**

The Infrared spectra were performed in a Bruker FT"IR model IFS66 spectrometer. Each compound was dispersed in KBr and pressed into a disc.IR spectra were.

Photoluminescence spectra were collected using a FLUOROLOG3 ISA/Jobin-Yvon spectrofluorometer equipped with Hamamatsu R928P photomultiplier a SPEX 1934 D phosphorimeter and Xenon pulsed-lamp of 150 W of power. Lifetime measurements were acquired by monitoring the maxima emission at 440, 545 and 615 nm for the ligand residues, $Tb^{3+}$ and $Eu^{3+}$ ions respectively.

The structure of $[Ln_2(Mell)(H_2O)_8]$ and crystal fragments of *RB-MOF*, *RG-MOF* and *RGB-MOF* was indexed by X-ray diffraction.The X-ray measurements were carried out in a Bruker SMART CCD APEX II area detector diffractometer with graphite-monochromated Mo *K*a radiation ($\lambda$ = 0.71073 Å) at room temperature (*T* = 293 K).

X-ray powder diffraction analyses were performed at room temperature, using a Bruker D8 Advanced with Davinci design equipped with a LynxEye Linear Position Sensitive Detector and a Copper (Cu) sealed tube ($\lambda k\alpha_1$ = 1.5404 Å, $\lambda k\alpha_2$ = 1.5444 Å, $I\alpha_2/I\alpha_1$ = 0.5). Intensity data were collected in step scanning mode, in the range from 5 to 50° (2θ), with a step size of 0.01°, Soller slit with 2.5° of divergence, 0.5° scattering slit and 0.6 mm receiving slit. FT-IR spectra were recorded from KBr pellets (in the 400-4000 $cm^{-1}$ spectral range) using a BRUKER IFS 66. Thermogravimetry–differential thermal analysis (TG–DTA) curves were acquired through a SHIMADZU DTG-60H instrument in the range from 25˚C to 900˚C using an alumina crucible with ca. 8.0 mg of samples, under dynamic nitrogen atmosphere (50 ml·min-1) and with a heating rate of 10º C·$min^{-1}$. The fluorescence microscopy images were obtained under a microscope Ollympus model BX51TF using a filter autofluorescence 330-385 nm. The images of the BRG-MOF and BGR-MOF were obtained from cross-sectional of crystals.

**Table S1.** X-ray diffraction data collection and refinement parameters for $[Eu_2(Mell)(H_2O)_8]$, $[Tb_2(Mell)(H_2O)_8]$ and $[Gd_2(Mell)(H_2O)_8]$, *R-MOF*, *G-MOF* and *B-MOF*, respectively.

| | **$[Eu_2(Mell)(H_2O)_8]$** | **$[Gd_2(Mell)(H_2O)_8]$** | **$[Tb_2(Mell)(H_2O)_8]$** |
|---|---|---|---|
| Chemical formula | $C_6H_{10}O_{11}Eu$ | $C_6H_{10}O_{11}Gd$ | $C_6H_{10}O_{11}Tb$ |
| M (g mol$^{-1}$) | 410.10 | 415.39 | 417.06 |
| Crystal system | Monoclinic | Monoclinic | Monoclinic |
| Space group | $P2_1/n$ | $P2_1/n$ | $P2_1/n$ |
| Unit cell *a* (Å) | 8.501(5) | 8.461(9) | 8.455(2) |
| *b* (Å) | 13.143(7) | 13.127(16) | 13.105(4) |
| *c* (Å) | 9.529(5) | 9.485(11) | 9.488(2) |
| $\beta$ | 94.682(2) | 94.652(7) | 94.439(10) |
| *V* (Å$^3$) | 1061.21(10) | 1050.1(2) | 1048.15(5) |
| Z | 4 | 4 | 4 |
| $D_c$ /g cm$^{-3}$ | 2.567 | 2.627 | 2.643 |
| Index ranges | $-10 \le h \le 10$ | $-10 \le h \le 10$ | $-10 \le h \le 10$ |
| | $-13 \le k \le 16$ | $-15 \le k \le 9$ | $-15 \le k \le 16$ |
| | $-11 \le l \le 11$ | $-11 \le l \le 11$ | $-11 \le l \le 11$ |
| Absorption coefficient /mm$^{-1}$ | 5.968 | 6.374 | 6.805 |
| Absorption correction | multi-scan | multi-scan | multi-scan |
| Max/min transmission | 0.3786 / 0.2457 | 0.7200 / 1.000 | 0.1819 / 0.1340 |
| Measured reflections | 9743 | 5420 | 9433 |
| Independent reflections / $R_{int}$ | 2181 / 0.0397 | 1848 / 0.0202 | 2142 / 0.0418 |
| Refined parameters | 170 | 187 | 180 |
| R1 (F) / wR2 ($F^2$) ($I > 2\sigma(I)$) | 0.0223 / 0.0512 | 0.0186 / 0.0453 | 0.0303 / 0.0777 |
| GooF | 1.065 | 1.152 | 1.123 |
| Largest diff.peak and hole (eÅ$^{-3}$) | 1.056 and -1.009 | 0.889 and -0.567 | 1.619 and -2.151 |
| Deposit number CCDC | 978276 | 888521 | 978277 |

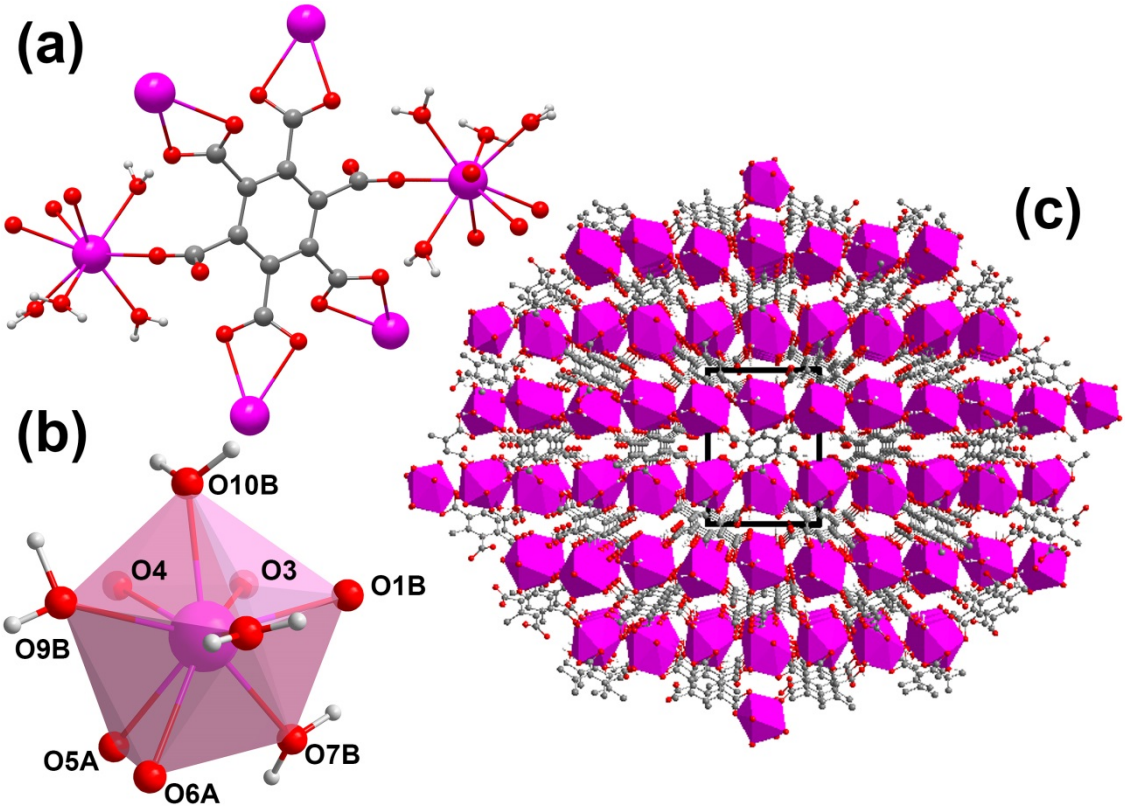


**Figure S2:** (a) Coordination environment of Mell anion; (b) Coordination polyhedron of $Ln^{3+}$; (c) 3D structure of $[Ln_2(Mell)(H_2O)_8]$. Pink sphere: $Ln^{3+}$ ion; Red sphere: Oxygen atom; Gray sphere: Carbon atom; Light Gray sphere: Hydrogen atom.

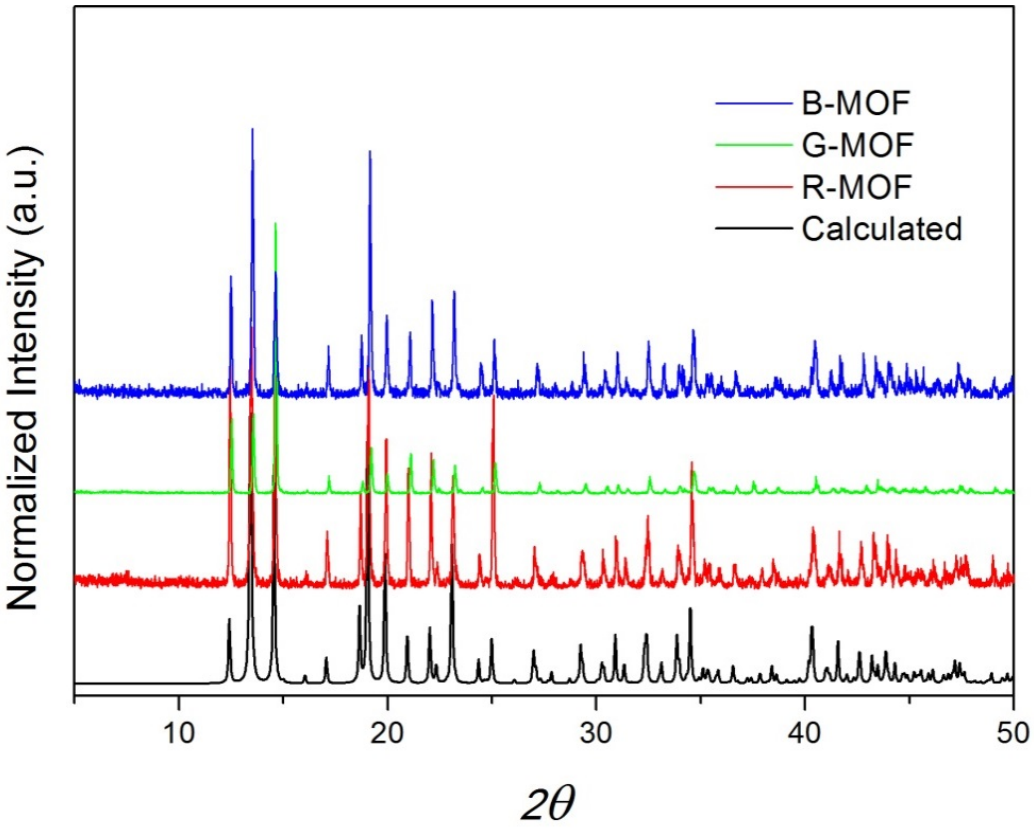


**Figure S3:** X-ray powder patterns. Calculated (black solid line), *R-MOF* (red solid line), *G-MOF* (green solid line) and *B-MOF* (blue solid line).

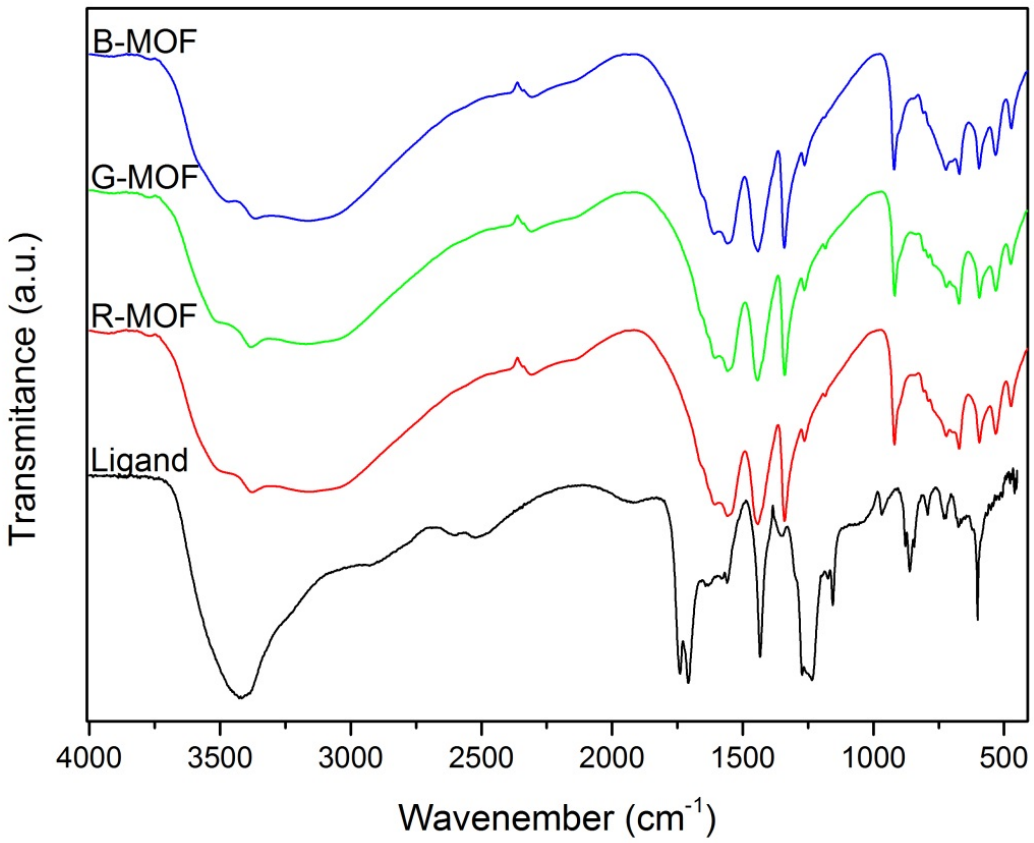


**Figure S4:** IR spectra. Mellitic acid (black solid line); *R-MOF* (red solid line); *G-MOF* (green solid line); *B-MOF* (blue solid line).

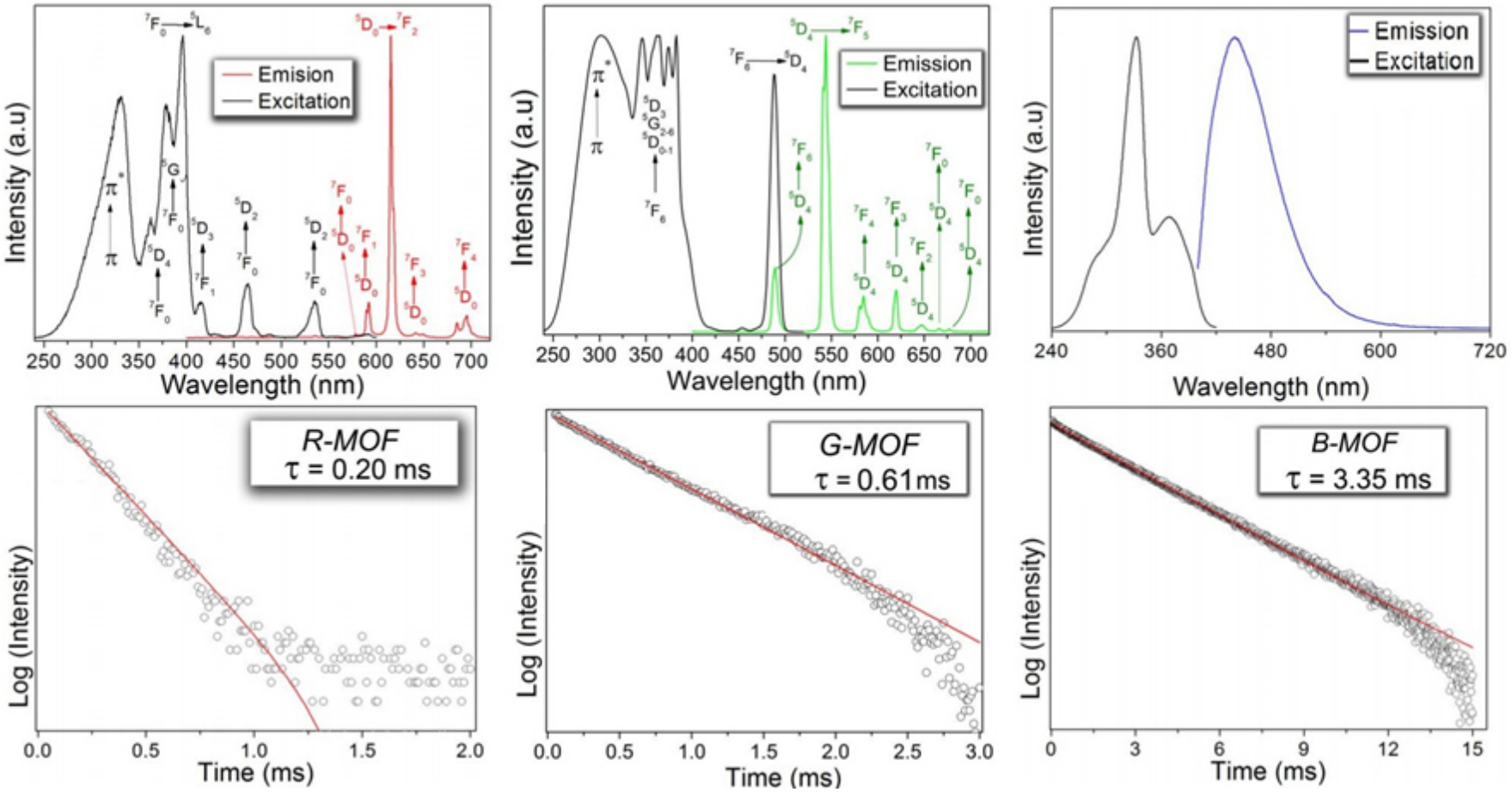


**Figure S5:** Excitation and emission spectra of *R-MOF* (A), *G-MOF* (B), *B-MOF* (C) and respectively normalized decay curves (D), (E) and (F). The decay curve (log scale) obtained upon excitation at 395 nm monitoring the emission at *ca.* 615 nm (*R-MOF*) and excitation at 378 nm monitoring the emission at *ca.* 545 nm (G-MOF) and excitation at 333 nm monitoring the emission at *ca.* 440 nm (*B-MOF*).

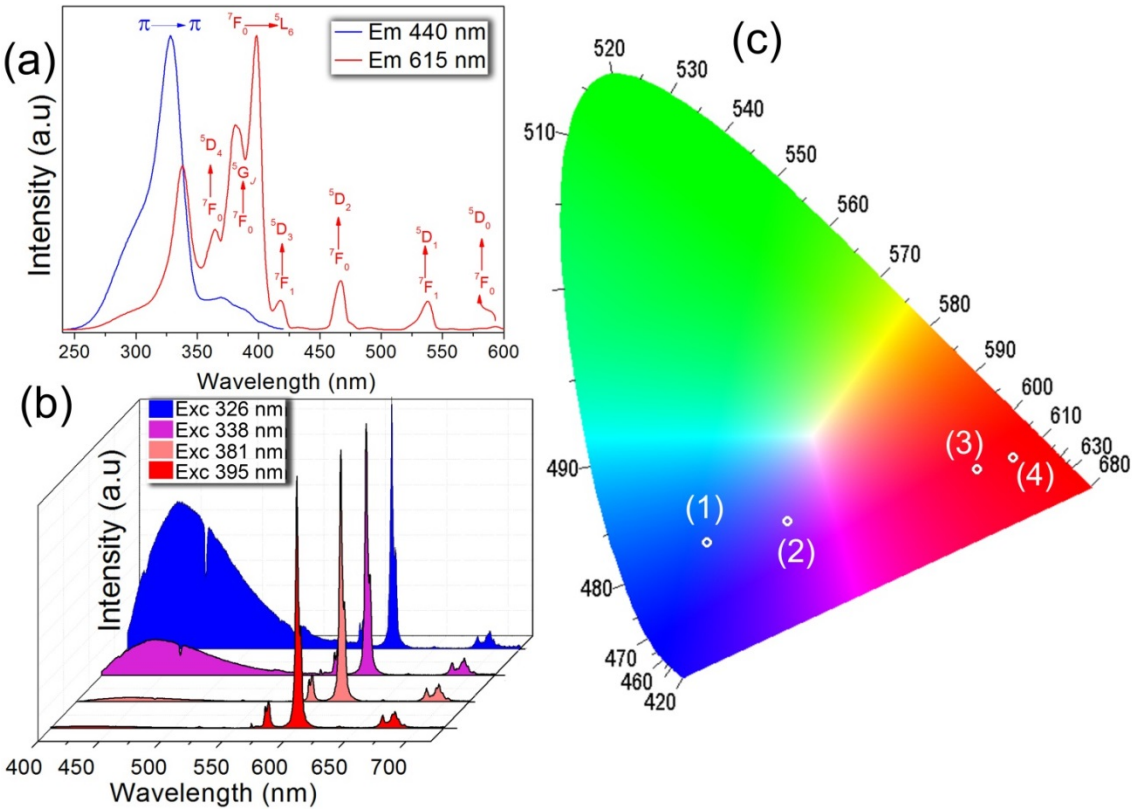


**Figure S6**. (a) Excitation spectra of *RB-MOF* obtained by monitoring of the ligand emission (440 nm, solid blue line) and $Eu^{3+}$ $^5D_0 \rightarrow {}^7F_2$ transition (615 nm, solid red line). (b) Emission spectra upon excitation at 328, 338, 381 and 395 nm. (c) CIE chromaticity diagram: (1) $\lambda_{exc}$ = 326 nm; (2) $\lambda_{exc}$ = 338 nm; (3) $\lambda_{exc}$ = 381nm; (4) $\lambda_{exc}$ = 395 nm.

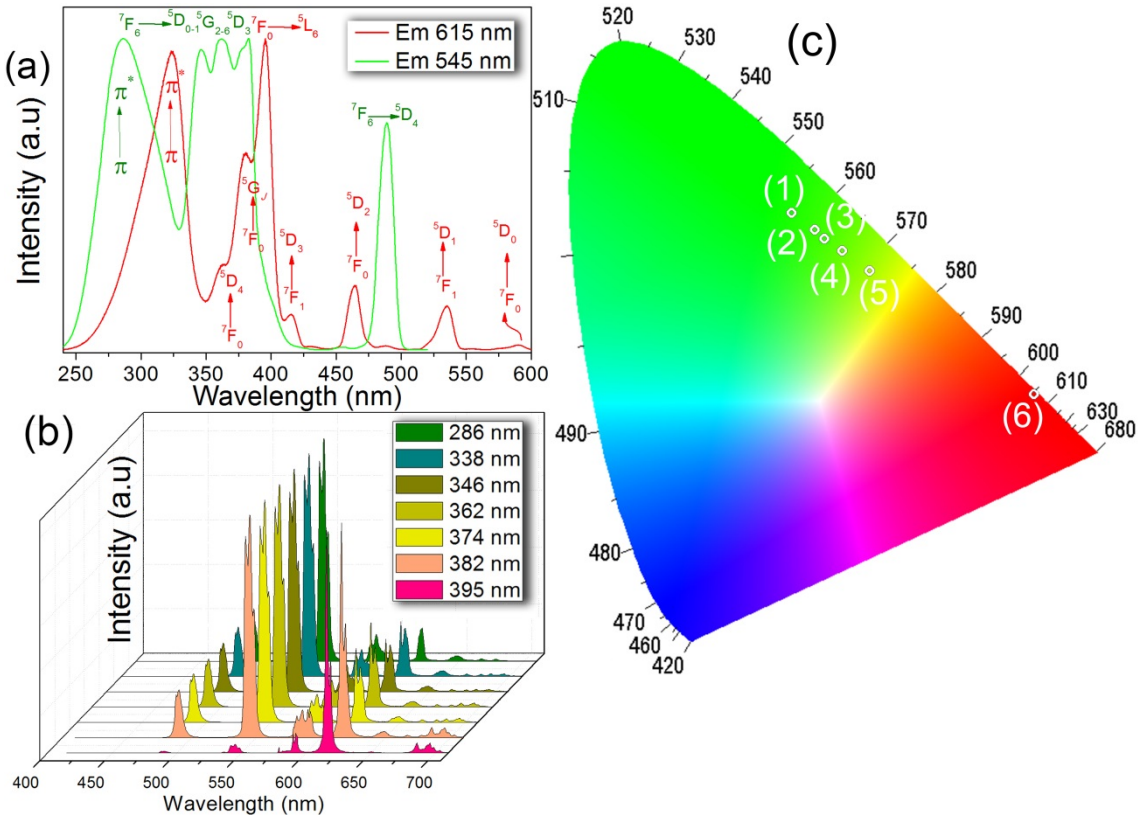


**Figure S7.** (a) Excitation spectra of *RG-MOF* acquired by monitoring $Tb^{3+}$ $^5D_4 \rightarrow {}^7F_5$ transition (545 nm, solid green line) and $Eu^{3+}$ $^5D_0 \rightarrow {}^7F_2$ transition (615 nm, solid red line). (b) Emission spectra upon excitation in 288, 338, 346, 374, 362, 382 and 395nm. (c) CIE chromaticity diagram: (1) $\lambda_{exc}$ = 286 nm; (2) $\lambda_{exc}$ = 338 and 346 nm; (3) $\lambda_{exc}$ = 374 nm; (4) $\lambda_{exc}$ = 362 nm, (5) $\lambda_{exc}$ = 382 nm and (6) $\lambda_{exc}$ = 395 nm.

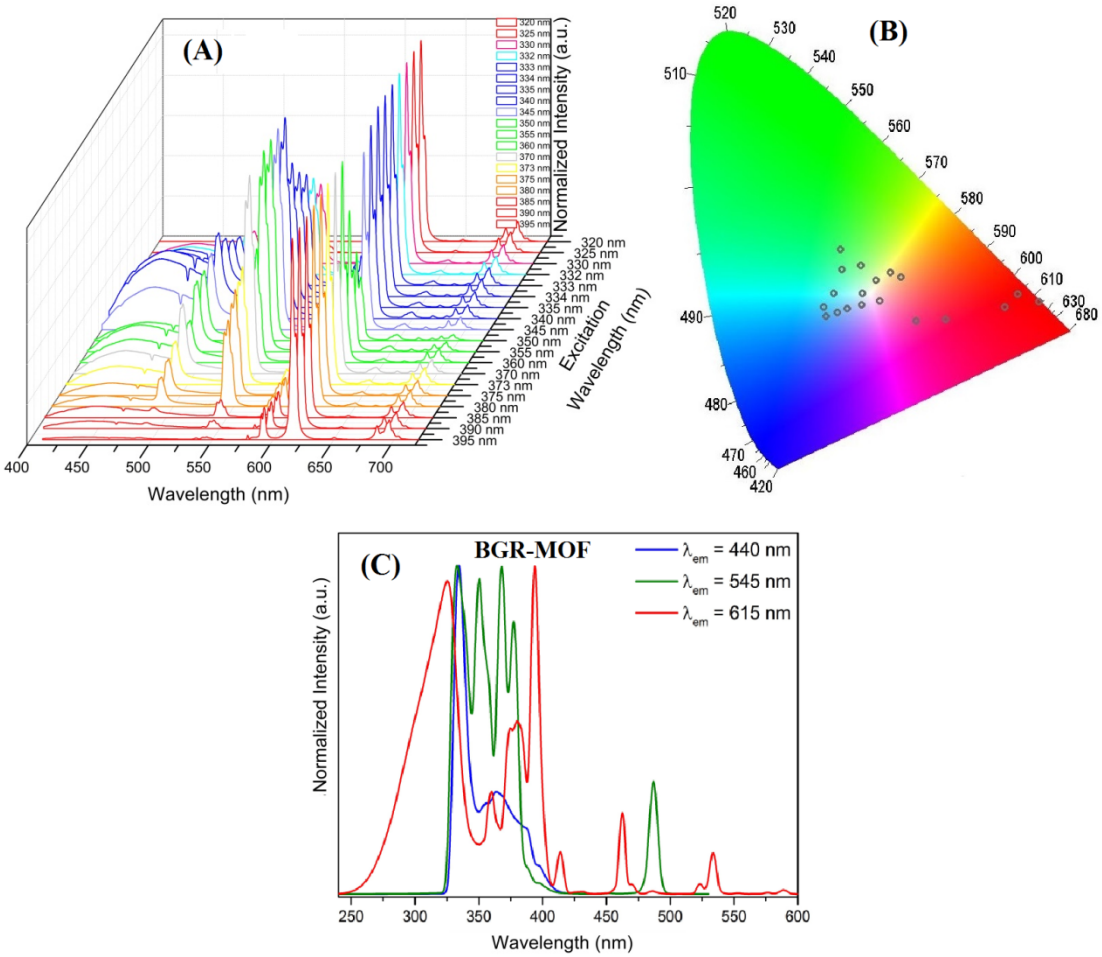


**Figure S8**: **(A)** Emission spectra of *BGR-MOF* upon excitation in 320 nm, 325 nm, 330 nm, 332 nm, 333 nm, 334 nm, 335 nm, 340 nm, 345 nm, 350 nm, 355 nm, 360 nm, 370 nm, 373 nm, 375 nm, 380 nm, 385 nm, 390 nm and 395nm. **(B)** CIE chromaticity diagram containing the colors of photoluminescence corresponding to each emission spectra in (A).**(C)** Excitation spectra were acquired by monitoring of the ligand emission (440 nm, solid blue line) and $Tb^{3+}$ $^5D_4 \rightarrow {}^7F_5$ transition (545 nm, solid green line) and $Eu^{3+}$ $^5D_0 \rightarrow {}^7F_2$ transition (615 nm, solid red line).

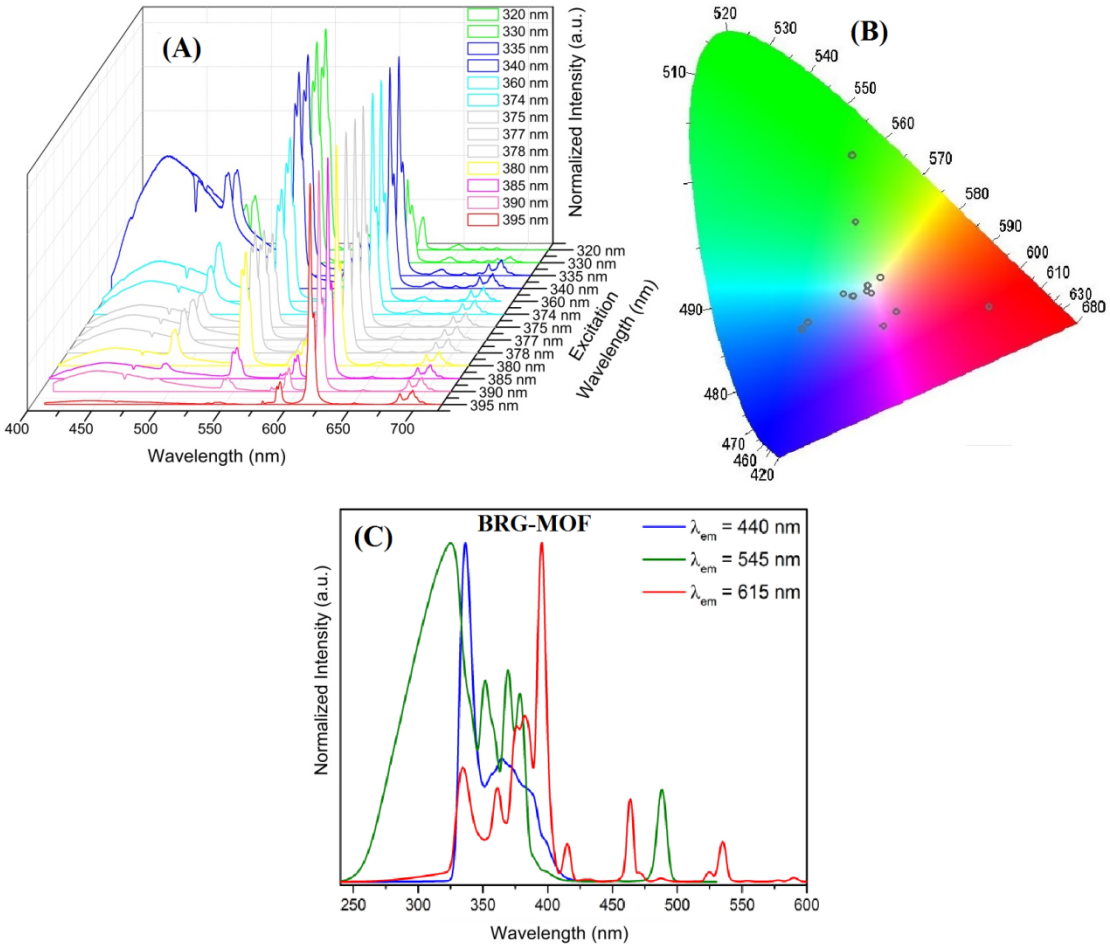


**Figure S9: (A)** Emission spectra of BRG-MOF upon excitation in 320 nm, 330 nm, 335 nm, 340 nm, 360 nm, 374 nm, 375 nm, 377 nm, 378 nm, 380 nm, 385 nm, 390 nm and 395nm. **(B)** CIE chromaticity diagram containing the photoluminescence colors corresponding to each emission spectra in (A). **(C)** Excitation spectra were acquired by monitoring of the ligand emission (440 nm, solid blue line) and $Tb^{3+}$ $^5D_4 \rightarrow {}^7F_5$ transition (545 nm, solid green line) and $Eu^{3+}$ $^5D_0 \rightarrow {}^7F_2$ transition (615 nm, solid red line).

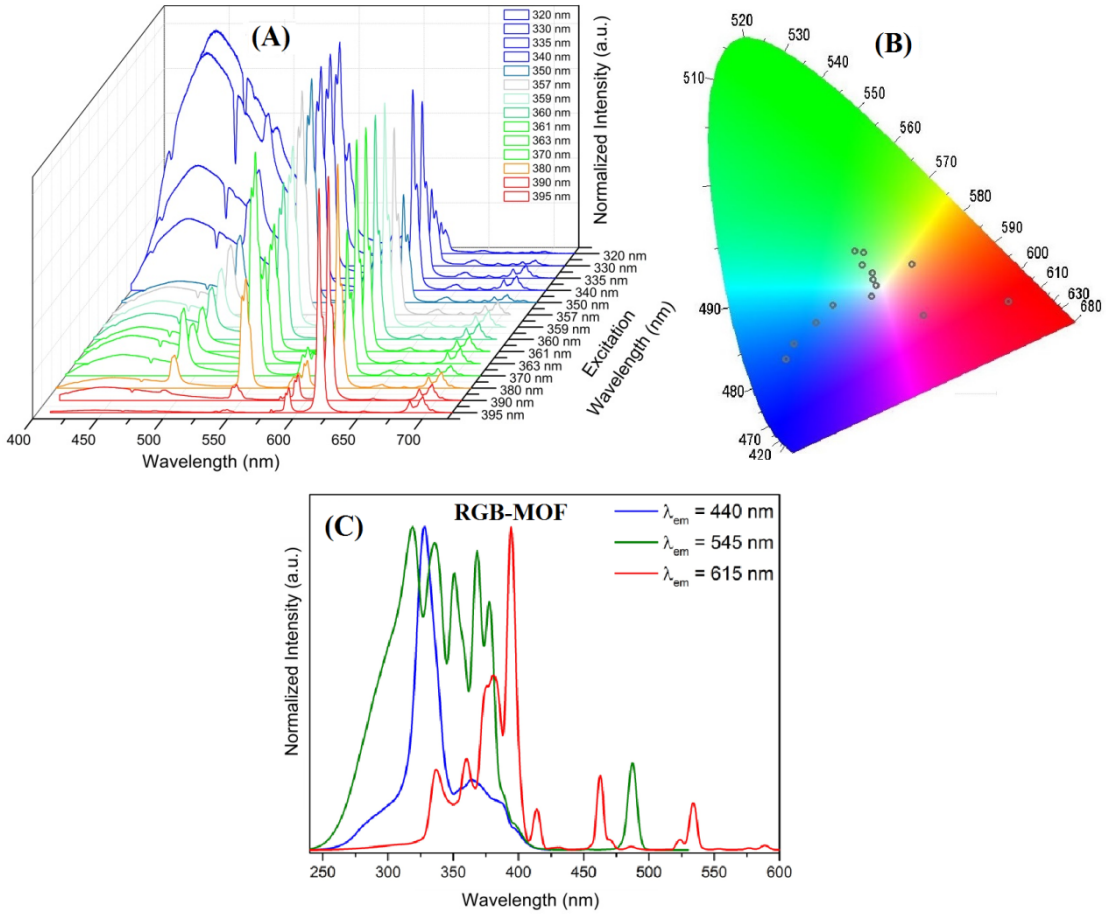


**Figure S10: (A)** Emission spectra of *RGB-MOF* upon excitation in 320 nm, 330 nm, 335 nm, 340 nm, 350 nm, 357 nm, 359 nm, 360 nm, 361 nm, 363 nm, 370 nm, 380 nm, 390 nm and 395nm. **(B)** CIE chromaticity diagram containing the photoluminescence colors corresponding to each emission spectra in (A). **(C)** Excitation spectra were acquired by monitoring of the ligand emission (440 nm, solid blue line) and $Tb^{3+}$ $^5D_4 \rightarrow {}^7F_5$ transition (545 nm, solid green line) and $Eu^{3+}$ $^5D_0 \rightarrow {}^7F_2$ transition (615 nm, solid red line).

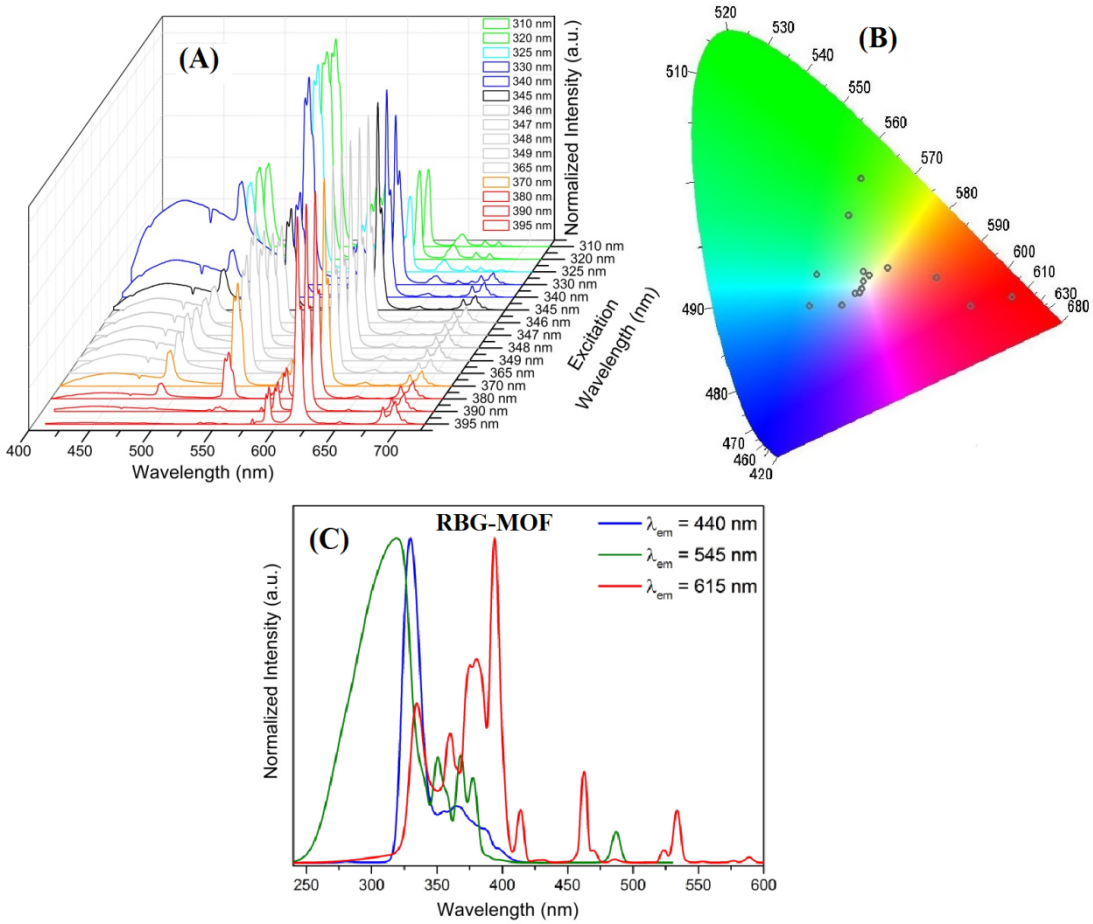


**Figure S11: (A)** Emission spectra of *RBG-MOF* upon excitation in 310 nm, 320 nm, 325 nm, 330 nm, 340 nm, 345 nm, 346 nm, 347 nm, 348 nm, 349 nm, 365 nm, 370 nm, 380 nm, 390 nm and 395nm. **(B)** CIE chromaticity diagram containing the photoluminescence colors corresponding to each emission spectra in (A). **(C)** Excitation spectra were acquired by monitoring of the ligand emission (440 nm, solid blue line) and $Tb^{3+}$ $^5D_4 \rightarrow {}^7F_5$ transition (545 nm, solid green line) and $Eu^{3+}$ $^5D_0 \rightarrow {}^7F_2$ transition (615 nm, solid red line).

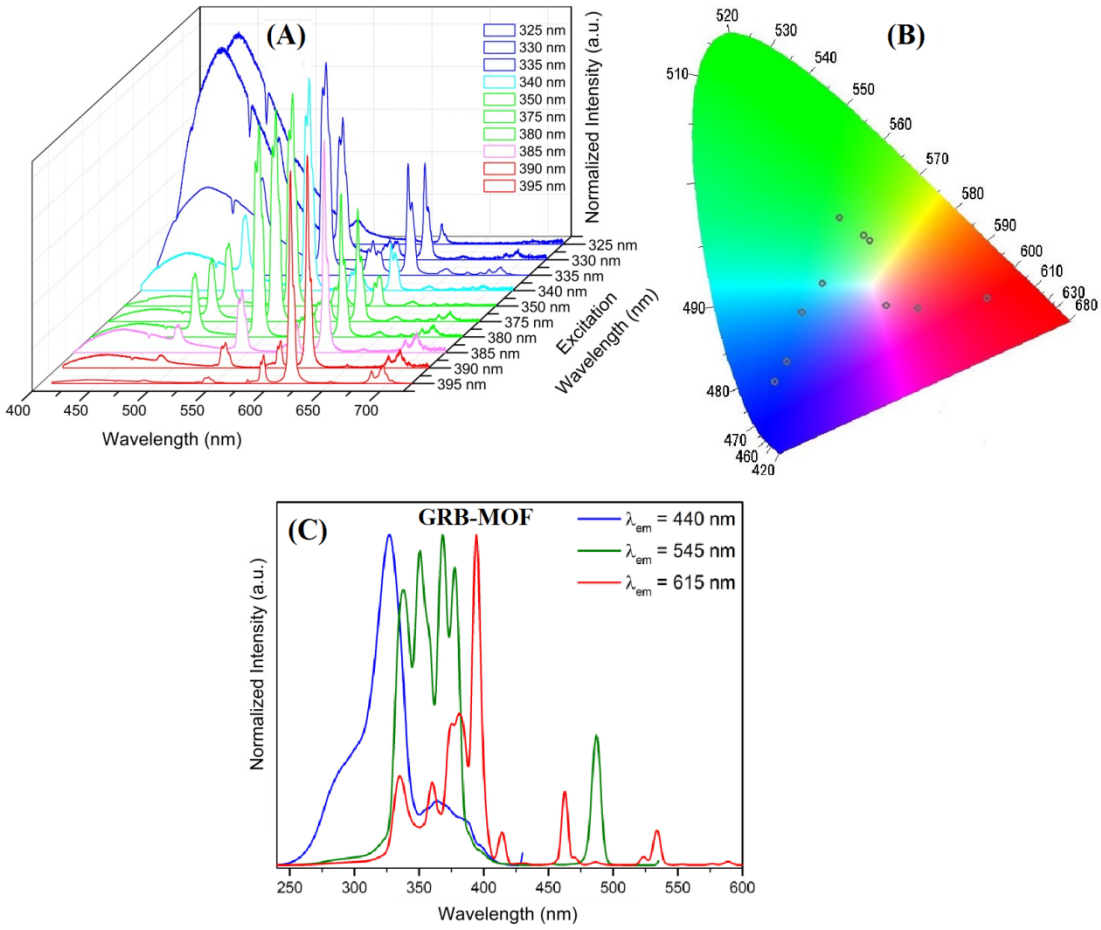


**Figure S12: (A)** Emission spectra of *GRB-MOF* upon excitation in 325 nm, 330 nm, 335 nm, 340 nm, 350 nm, 375 nm, 380 nm, 385 nm, 390 nm and 395nm. **(B)** CIE chromaticity diagram containing the photoluminescence colors corresponding to each emission spectra in (A). **(C)** Excitation spectra were acquired by monitoring of the ligand emission (440 nm, solid blue line) and $Tb^{3+}$ $^5D_4 \rightarrow {}^7F_5$ transition (545 nm, solid green line) and $Eu^{3+}$ $^5D_0 \rightarrow {}^7F_2$ transition (615 nm, solid red line).

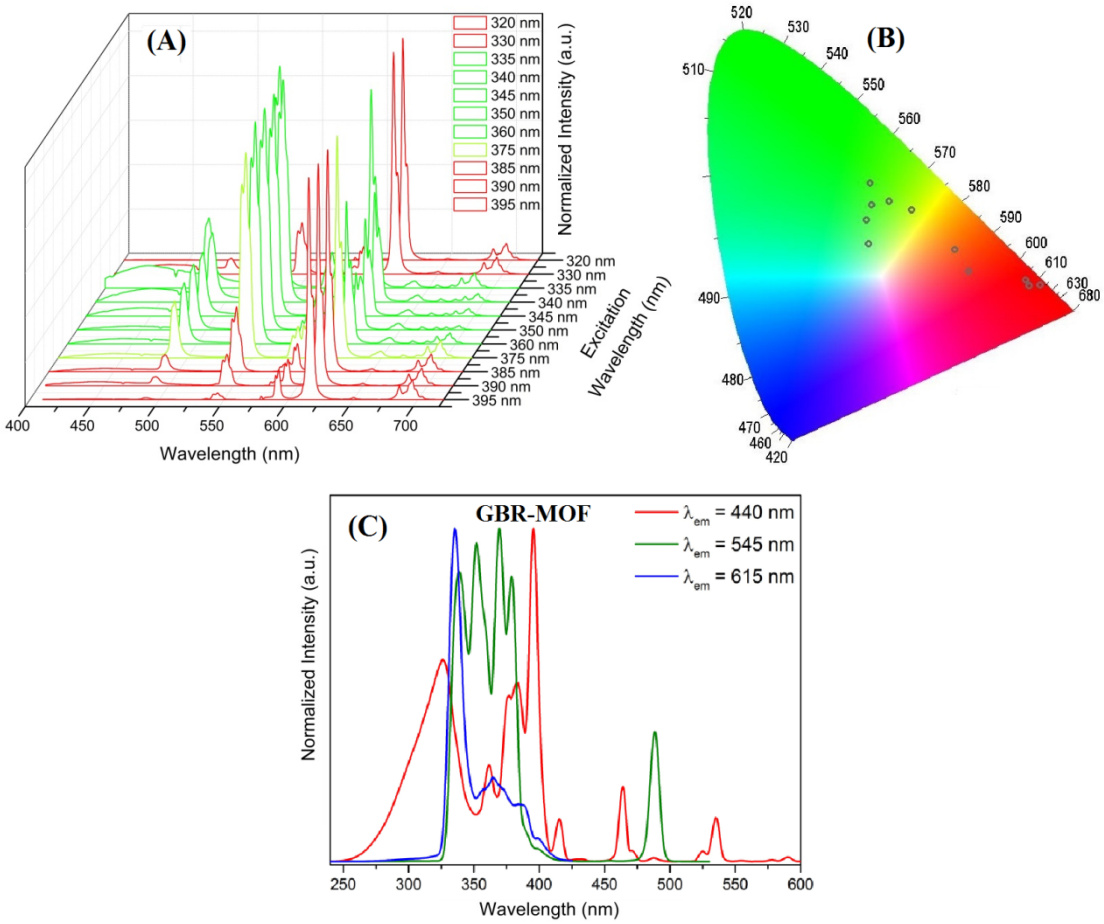


**Figure S13: (A)** Emission spectra of *GBR-MOF* upon excitation in 320 nm, 330 nm, 335 nm, 340 nm, 345 nm, 350 nm, 360 nm, 375 nm, 385 nm, 390 nm and 395nm. **(B)** CIE chromaticity diagram containing the photoluminescence colors corresponding to each emission spectra in (A). **(C)** Excitation spectra were acquired by monitoring of the ligand emission (440 nm, solid blue line) and $Tb^{3+}$ $^5D_4 \rightarrow {}^7F_5$ transition (545 nm, solid green line) and $Eu^{3+}$ $^5D_0 \rightarrow {}^7F_2$ transition (615 nm, solid red line).

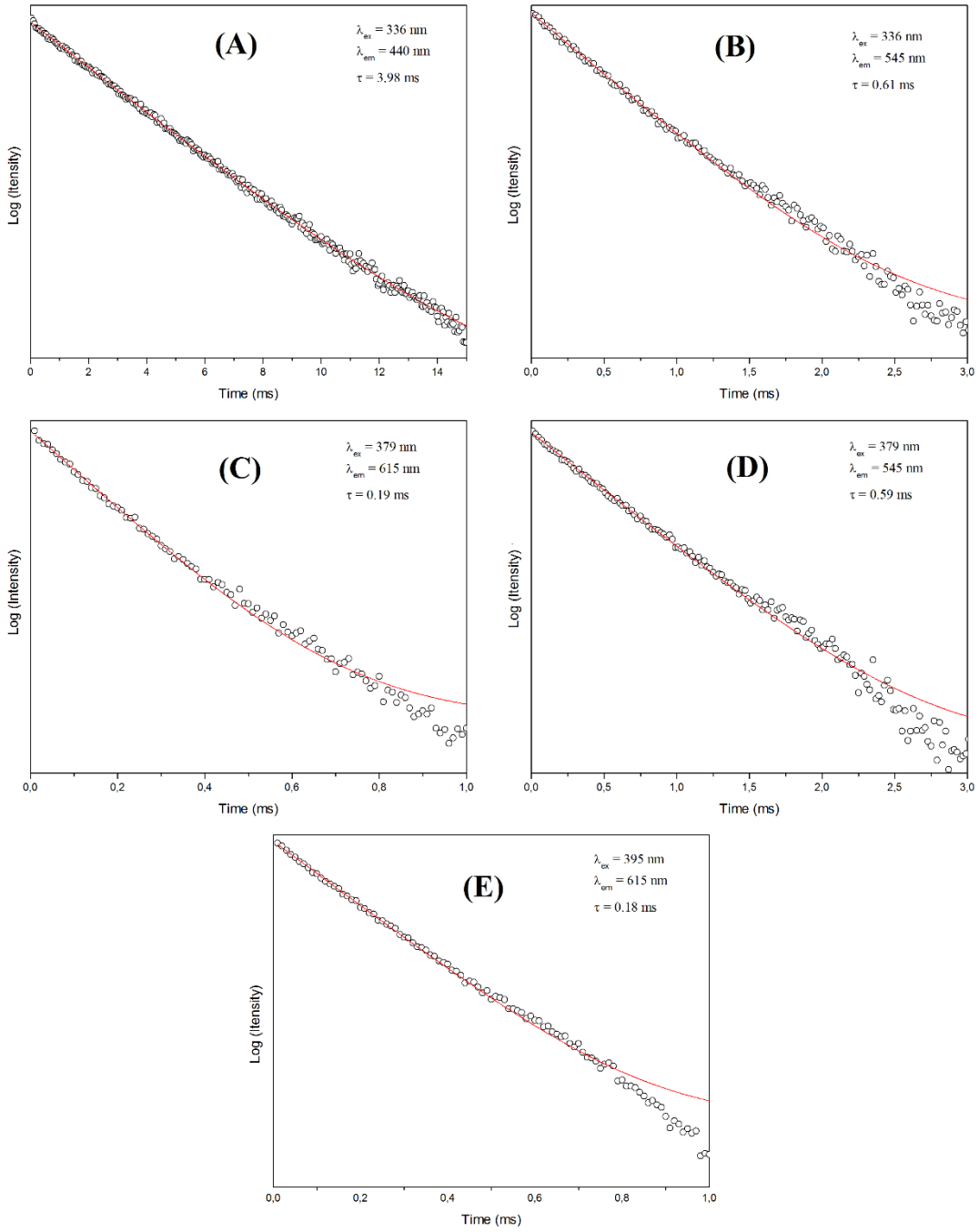


**Figure S14:** Normalized decay curves of *BGR-MOF* upon excitation at 336 nm and by monitoring of the ligand emission ca. 440 nm (A) and $Tb^{3+}$ $^5D_4 \rightarrow {}^7F_5$ transition at *ca.* 545 nm (B) and upon excitation at 379 nm and by monitoring the $Tb^{3+}$ $^5D_4 \rightarrow {}^7F_5$ transition at *ca.* 545 nm (D) and $Eu^{3+}$ $^5D_0 \rightarrow {}^7F_2$ transition at *ca.* 615 nm (C) and upon excitation at 395 nm and by monitoring the $Eu^{3+}$ $^5D_0 \rightarrow {}^7F_2$ transition at *ca.* 615 nm(E).

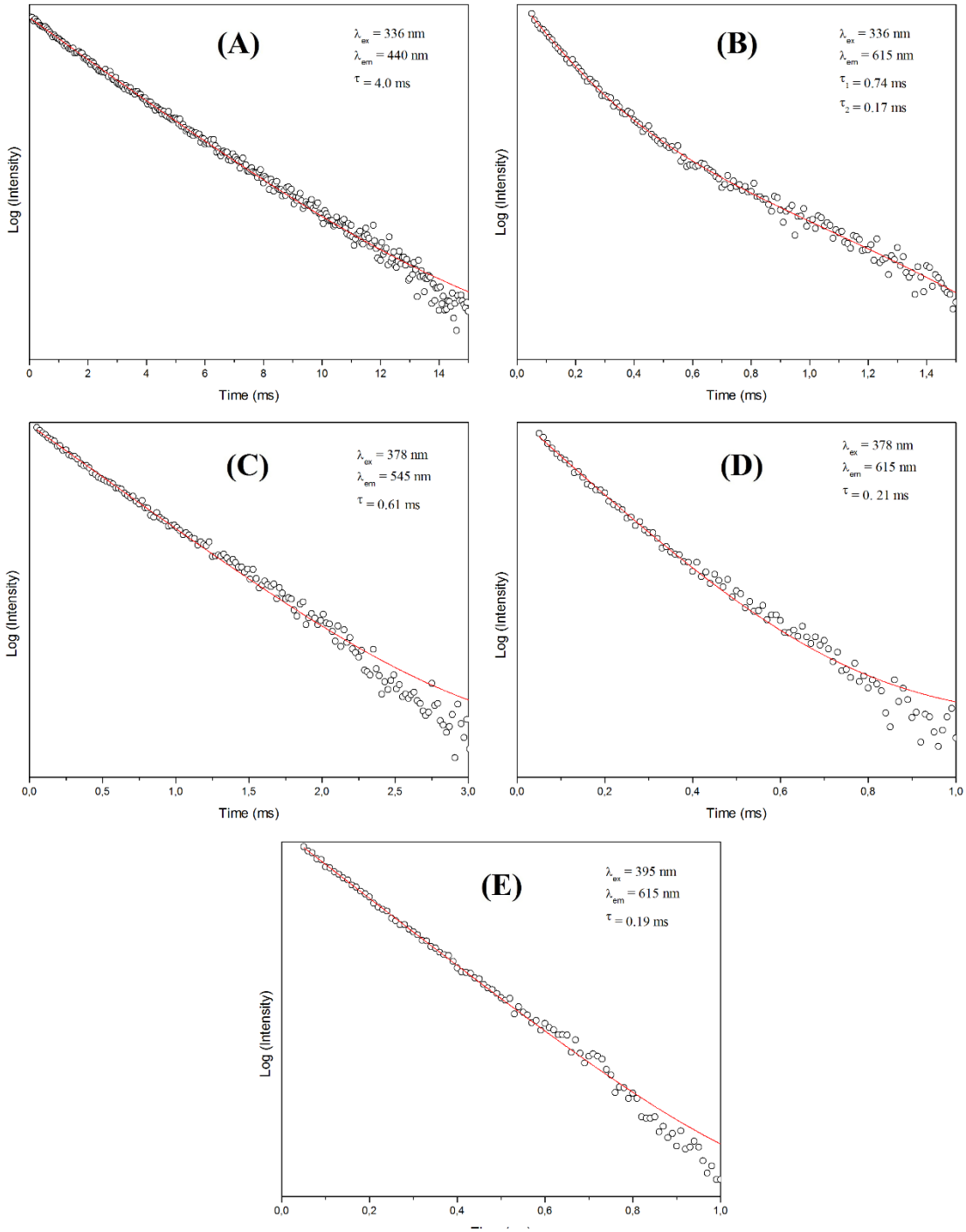


**Figure S15:** Normalized decay curves of *BRG-MOF* upon excitation at 336 nm and by monitoring of the ligand emission ca. 440 nm(A) and $Eu^{3+}$ $^5D_0 \rightarrow {}^7F_2$ transition at *ca.* 615 nm (B) and upon excitation at 378 nm and by monitoring the $Tb^{3+}$ $^5D_4 \rightarrow {}^7F_5$ transition at *ca.* 545 nm (C) and $Eu^{3+}$ $^5D_0 \rightarrow {}^7F_2$ transition at *ca.* 615 nm (D) and upon excitation at 395 nm and by monitoring the $Eu^{3+}$ $^5D_0 \rightarrow {}^7F_2$ transition at *ca.* 615 nm (E).